Frequency Invariant Beampatterns for Wideband Synthetic Aperture Channel Sounders

Peter Vouras
Wireless Networks Division, National Institute of Standards and Technology, Gaithersburg, MD

Jeanne Quimby, Benjamin Jamroz, Alec Weiss, Rodney Leonhardt, Dylan F. Williams, Kate A. Remley
RF Technology Division, National Institute of Standards and Technology, Boulder, CO

***Abstract*—This paper derives two novel frequency invariant beamformers (FIBs) for use with wideband synthetic aperture channel sounders. Results using measured data show that the choice of beampattern can affect the amount of diffuse multipath energy received through the array sidelobes and influence the estimated channel impulse and frequency responses.**

***Index Terms*—synthetic aperture, diffuse multipath, fading, frequency invariant beamformer, wireless system**

I. Introduction

Precise measurement and characterization of millimeter wave channels requires antennas capable of high angular resolution to resolve closely spaced multipath sources. To achieve angular resolution on the order of a few degrees, these antennas must be electrically large, which is impractical for hardware arrays at high frequencies [1]. An alternative approach is to synthesize a virtual aperture in space by using an accurate mechanical positioner or robot to move a receive antenna along points on a sampling grid. An advantage of creating virtual apertures is that the receive signal is digitized at every spatial sample position, which enables the use of sophisticated angle of arrival estimation methods and adaptive beamforming techniques. The main contributions of this paper are two novel frequency invariant beamformers (FIBs) that can be employed with wideband synthetic aperture channel sounders. The first beamformer presented is for a pencil beam with constant beamwidth versus frequency and greatly reduced sidelobes that can be employed in scenarios that require maximum available angular resolution. This paper extends the derivation of an analytic solution introduced in [2] from nonlinear beamforming to a linear beamformer. The second beamformer is a novel linear program for designing symmetric flat top beampatterns centered at boresight. This beampattern is most useful for measuring multipath fading characteristics over a wide angular sector. Both algorithms differ from wideband beamformers that jointly optimize the array spatial and frequency responses or techniques that utilize synthetic beamwidths to excise detections from unwanted directions [3]–[5].

Results presented were derived using data collected on a 35-by-35 planar spatial sample grid with the distance between samples equal to 3.7 mm or one-half wavelength at 40 GHz. A vector network analyzer connected between the transmit and receive antennas was used to measure S21 parameters in 10 MHz increments between 26.5 and 40 GHz which corresponds to a 13.5 GHz synthesized bandwidth and 1,351 frequency samples. The maximum unambiguous signal duration that can be measured is equal to the reciprocal of the frequency increment.

II. Frequency and Scanning Behavior of the Array Factor

The far-field response in spherical coordinates (θ, ϕ) for an array of $M \times N$ homogeneous elements located in the xy plane is given by,

$$B(\theta,\phi) = E(\theta,\phi) \sum_{m=0}^{M-1} \sum_{n=0}^{N-1} w_{mn} e^{jk(x_m \sin\theta\cos\phi + y_n \sin\theta \sin\phi)} \tag{1}$$

where $E(\theta,\phi)$ is the array element pattern, the wavenumber $k = 2\pi/\lambda$, λ is the operating wavelength, and w_{mn} is the array element weighting. If the array elements are uniformly spaced on a rectangular grid then the element locations are given by $x_m = md_x$ and $y_n = nd_y$ where d_x and d_y denote the spacing between elements in the x and y directions. This equation can be rewritten as a 2-D spatial Fourier Transform by using sine space coordinates $u = \sin\theta\cos\phi$ and $v = \sin\theta\sin\phi$ [6],

$$B(u,v) = E(u,v) \sum_{m=0}^{M-1} \sum_{n=0}^{N-1} w_{mn} e^{jk(md_x u + nd_y v)}. \tag{2}$$

The summation term is known as the array factor. The array factor repeats in the u dimension with period λ/d_x and repeats in the v dimension with period λ/d_y. A single period in uv space of the array factor is equal to the rectangular region $-0.5\lambda/d_x \le u < 0.5\lambda/d_x$ and $-0.5\lambda/d_y \le v < 0.5\lambda/d_y$. The visible region of the array factor that exists in physical space corresponds to the interior of the unit circle $u^2 + v^2 \le 1$. The large peaks outside the unit circle are known as grating lobes. The Nyquist spatial sampling rate that avoids spatial aliasing or grating lobes is given by $d_x = d_y = \lambda/2$. If the element spacing is greater than $\lambda/2$ then the array is undersampled and the grating lobes move closer to the unit circle and may even enter the visible region. If the element spacing is less than $\lambda/2$ then the array is oversampled and the grating lobes move farther away from the unit circle. Fig. 1 illustrates the output (dB scale) of a spatial Fourier Transform and the array factor at 40 GHz for

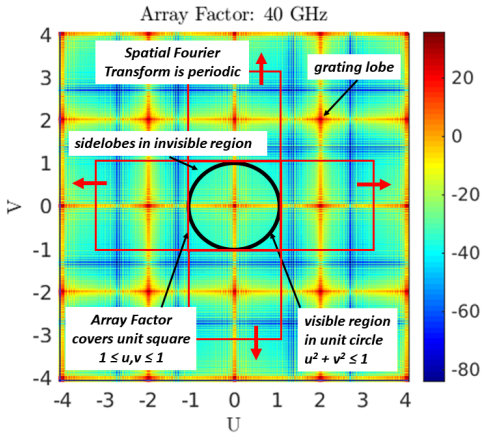

Fig. 1. Spatial Fourier Transform Output and Array Factor: 40 GHz.

a 35-by-35 planar aperture. The inter-element spacing in the x and y directions is equal to $\lambda/2$ at 40 GHz or 3.7 mm. With the spacing held fixed, the array is oversampled at 26.5 GHz so the grating lobes move farther away from the visible region. The peak of the main beam depends only on the number of array elements and is equal to $10log_{10}(MN)$ or 30.8 dB.

All of the properties of Fourier Transforms apply to the array factor and in particular the Fourier shift and the Fourier scaling properties. The Fourier shift property is relevant when the main beam is steered to a direction (u_0, v_0). Beam steering is accomplished by applying the linear phase taper $e^{-jk(md_x u_0 + nd_y v_0)}$ across the aperture. The main beam will shift by an angular distance equal to the slope of the linear phase taper in the u and v directions. Steering the main beam for a single frequency is a linear transformation that does not affect the amplitude of the array factor or the shape of the main beam. When the beam scans, sidelobes that were originally outside the unit circle in the invisible region of uv space will enter the visible region and therefore the sidelobe structure of the beam changes.

In wideband regimes where the linear phase taper is computed for a single center frequency but applied to the aperture over a wider bandwidth, then the main beam will squint, or point to different directions as the operating frequency changes. Beam squint is an undesired effect that can be mitigated by using true time delay beam steering or a frequency invariant beamformer [6]. True time delay beam steering applies a frequency independent time delay or a frequency dependent linear phase shift between array elements to steer the beam and can be easily implemented on synthetic apertures.

The Fourier scaling property states that changing the sample spacing of a 2D discrete sequence $h(m,n)$ expands or contracts the output of the Fourier transform $H(u,v)$ according to

$$H(\frac{u}{a}, \frac{v}{b}) \iff \frac{1}{|ab|} h(am, bn). \tag{3}$$

This property implies that if the physical spacing between array elements is held fixed while the operating frequency decreases, then the width of every angular lobe in the beampattern (main beam and sidelobes alike) will increase. Conversely, if the element spacing is held fixed while the frequency increases, then the width of every angular lobe decreases. Consequently, a synthetic aperture of fixed dimensions attains higher angular resolution at 40 GHz than at 26.5 GHz due to the narrower width of the main beam (approximately equal to λ/D radians, where D is the largest dimension of the aperture in the principal planes) [6]. Fig. 2 illustrates the Fourier scaling property by comparing a u-dimension cut of the array beampattern for 26.5 and 40 GHz with the main beam steered to $(u = 0.4, v = 0.3)$. In channel sounding applications it is important to maintain a frequency invariant array response such that it does not obfuscate the estimated channel frequency response.

III. Wideband Power Angle Delay Profile (PADP)

As mentioned previously, true time delay beam steering can be implemented on synthetic apertures to avoid beam squint when the frequency varies. True time delay beam steering requires applying a frequency dependent phase taper to the array output vector to steer the beam in a desired direction. Next an Inverse Fourier Transform is computed after beamforming to recover the beam output in the delay domain, also known as a power delay profile (PDP). The process is summarized in Algorithm 1 below.

Algorithm 1 PADP Creation

Require: Array output vector $\mathbf{y}(\omega_k)$ at each frequency ω_k and desired beam pointing direction (u_0, v_0)

1: Compute the phase steering vector for each frequency, $\mathbf{w}(\omega_k; u_0, v_0)$.
2: Beamform the array output vector $\mathbf{y}(\omega_k)$ at each frequency by forming the dot product $b(\omega_k; u_0, v_0) = \mathbf{w}(\omega_k; u_0, v_0)^H \mathbf{y}(\omega_k)$
3: Compute the Inverse Fourier Transform (temporal) to obtain the beam output (directional PDP), $x(\tau_k; u_0, v_0) = IFT[b(\omega_k; u_0, v_0)]$
4: For a fixed delay, $\tau = \tau_0$, $x(\tau_0; u, v)$ is the spatial frequency spectrum of all signal sources impinging on the array and can be used to estimate angles of arrival

The frequency invariant beamformers proposed in this paper replace the phase steering vectors $\mathbf{w}(\omega_k; u_0, v_0)$ with optimized weight vectors computed at every frequency for the desired steering direction.

IV. Frequency Invariant Pencil Beam With Reduced Sidelobes

This beamformer satisfies a main beam constraint that specifies the desired pointing direction (u_0, v_0) while simultaneously minimizing the integrated sidelobe level of the adapted

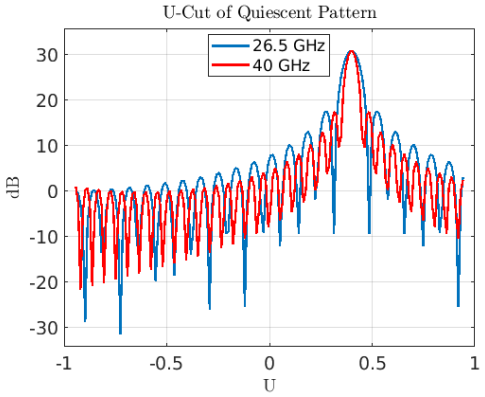

Fig. 2. Fourier Scaling Property: Beam Scanned to $(u = 0.4, v = 0.3)$.

antenna pattern for a fixed frequency ω_k. The array steering vector in a direction (u_j, v_j) is given by

$$\mathbf{s}(u_j, v_j) = \left[e^{-j\frac{2\pi}{\lambda_k}(md_x u_j + nd_y v_j)} \middle| \, m = 0, .., M-1, \;\; n = 0, .., N-1 \right]^T. \tag{4}$$

Steering vectors also form the basis functions of the spatial Fourier Transform in eqn. (2). In the sequel let N denote the total number of elements in the planar array to simplify notation. Define the desired width of the main beam region as $u^2 + v^2 \leq \mu$ where μ is a user defined radius. Angles outside the main beam region are defined to be in the sidelobe region. The objective function to be optimized is to minimize

$$J(\mathbf{w}) = \sum_{j=0}^{L-1} |\mathbf{w}^H \mathbf{s}(u_j, v_j)|^2 \tag{5}$$

such that

$$\mathbf{G}^H \mathbf{w} = [\mathbf{s}(u_0, v_0) | \mathbf{s}(u_1, v_1) | \ldots | \mathbf{s}(u_{K-1}, v_{K-1})]^H \mathbf{w} = \mathbf{b} \tag{6}$$

where the L angles (u_j, v_j) in the summation are sampled on a discrete grid in the sidelobe region of the antenna pattern. For the case of a single main beam constraint $K = 1$ and $\mathbf{b} = [1]$. Define the Hermitian matrix $\mathbf{Q}$ to be

$$\mathbf{Q} \equiv \sum_{j=0}^{L-1} \mathbf{s}(u_j, v_j) \mathbf{s}(u_j, v_j)^H \tag{7}$$

and the optimization program becomes

$$\begin{aligned} \text{minimize} \quad & J(\mathbf{w}) = \mathbf{w}^H \mathbf{Q} \mathbf{w} \\ \text{such that} \quad & \mathbf{G}^H \mathbf{w} = \mathbf{b}. \end{aligned} \tag{8}$$

The constraint matrix $\mathbf{G}$ has linearly independent columns. Note that the standard analytic solution $\mathbf{w}_{OPT} = \mathbf{Q}^{-1}\mathbf{G}[\mathbf{G}^H\mathbf{Q}^{-1}\mathbf{G}]^{-1}\mathbf{b}$ for quadratic functions with linear constraints is not applicable here because the marix $\mathbf{Q}$ is not necessarily full rank.

An analytic solution for the program in eqn. (8) will be derived using the method of Lagrange multipliers as described in [2] for a nonlinear beamformer. Adjoining the constraints in eqn. (8) to the objective function yields the real-valued Lagrangian

$$H(\mathbf{w}) = \tfrac{1}{2}\mathbf{w}^H \mathbf{Q} \mathbf{w} + \boldsymbol{\lambda}_R^T \Re e\{\mathbf{G}^H \mathbf{w} - \mathbf{b}\} + \boldsymbol{\lambda}_I^T \Im m\{\mathbf{G}^H \mathbf{w} - \mathbf{b}\}. \tag{9}$$

Minimizing the Lagrangian transforms the original optimization program with constraints into an unconstrained minimization. The optimum solution is obtained by taking the gradient of $H(\mathbf{w})$ with respect to the real and imaginary parts of $\mathbf{w} = \mathbf{w}_R + j\mathbf{w}_I$ and then setting the resulting quantities equal to zero. This step yields,

$$\begin{aligned} \frac{\partial H(\mathbf{w})}{\partial \mathbf{w}_R} &= \tfrac{1}{2}\mathbf{w}^H \mathbf{Q} + \boldsymbol{\lambda}_R^T \Re e\{\mathbf{G}^H\} + \boldsymbol{\lambda}_I^T \Im m\{\mathbf{G}^H\} = \mathbf{0} \\ \frac{\partial H(\mathbf{w})}{\partial \mathbf{w}_I} &= \tfrac{1}{2} j\mathbf{w}^H \mathbf{Q} - \boldsymbol{\lambda}_R^T \Im m\{\mathbf{G}^H\} + \boldsymbol{\lambda}_I^T \Re e\{\mathbf{G}^H\} = \mathbf{0} \end{aligned} \tag{10}$$

Defining the derivative of $H(\mathbf{w})$ with respect to $\mathbf{w}$ as

$$\frac{\partial H(\mathbf{w})}{\partial \mathbf{w}} = \frac{\partial H(\mathbf{w})}{\partial \mathbf{w}_R} - j\frac{\partial H(\mathbf{w})}{\partial \mathbf{w}_I} \tag{11}$$

and the complex $(K+1) \times 1$ Lagrange multiplier vector as $\boldsymbol{\lambda} = \boldsymbol{\lambda}_R + j\boldsymbol{\lambda}_I$ yields

$$\mathbf{Q}\mathbf{w} = -\mathbf{G}\boldsymbol{\lambda}. \tag{12}$$

Next the singular value decomposition (SVD) of $\mathbf{Q}$ is computed. The rank of $\mathbf{Q}$ is denoted r.

$$\mathbf{Q} = \begin{bmatrix} \mathbf{U}_1 & \mathbf{U}_2 \end{bmatrix} \begin{bmatrix} \boldsymbol{\Sigma} & \mathbf{0} \\ \mathbf{0} & \mathbf{0} \end{bmatrix} \begin{bmatrix} \mathbf{V}_1^H \\ \mathbf{V}_2^H \end{bmatrix}. \tag{13}$$

The matrix sizes are: $\mathbf{U}_1$ is $N^2 \times r$, $\mathbf{U}_2$ is $N^2 \times (N^2 - r)$, $\mathbf{V}_1$ is $N^2 \times r$, $\mathbf{V}_2$ is $N^2 \times (N^2 - r)$, and $\boldsymbol{\Sigma}$ is $r \times r$. The matrix $\mathbf{V}_1\mathbf{V}_1^H$ is the projection onto $N(\mathbf{Q})^\perp = R(\mathbf{Q}^H)$ and the matrix $\mathbf{V}_2\mathbf{V}_2^H$ is the projection onto $N(\mathbf{Q})$. Here, R denotes the range space of a matrix, N the null space, and $^\perp$ the orthogonal complement. Decomposing the weight vector $\mathbf{w}$ into

$$\mathbf{w} = \mathbf{V}_1 {\mathbf{V}_1}^H \mathbf{w} + \mathbf{V}_2 {\mathbf{V}_2}^H \mathbf{w} \tag{14}$$

and substituting into eqn. (12) produces

$$\mathbf{V}_1\mathbf{V}_1^H\mathbf{w} = -\mathbf{V}_1\boldsymbol{\Sigma}^{-1}\mathbf{U}_1^H\mathbf{G}\boldsymbol{\lambda}. \tag{15}$$

Since $\mathbf{Q}\mathbf{V}_2\mathbf{V}_2^H\mathbf{w} = \mathbf{0}$, the orthogonal component of $\mathbf{w}$, $\mathbf{V}_2\mathbf{V}_2^H\mathbf{w}$, does not contribute to the solution. Consequently, the optimal weight vector can now be set equal to

$$\mathbf{w}_{OPT} = -\mathbf{V}_1\boldsymbol{\Sigma}^{-1}\mathbf{U}_1^H\mathbf{G}\boldsymbol{\lambda}_{OPT} \tag{16}$$

where $\boldsymbol{\lambda}_{OPT}$ is the corresponding optimal Lagrange multiplier vector. Notice the matrix $\mathbf{V}_1\boldsymbol{\Sigma}^{-1}\mathbf{U}_1^H$ is the pseudoinverse of $\mathbf{Q}$. The vector $\boldsymbol{\lambda}_{OPT}$ is determined by applying the constraint equation $\mathbf{G}^H\mathbf{w} = \mathbf{b}$. In most practical applications, the $(K+1) \times (K+1)$ matrix $\mathbf{G}^H\mathbf{V}_1\boldsymbol{\Sigma}^{-1}\mathbf{U}_1^H\mathbf{G}$ is invertible so the final result becomes

$$\mathbf{w}_{OPT} = \mathbf{V}_1\boldsymbol{\Sigma}^{-1}\mathbf{U}_1^H\mathbf{G}[\mathbf{G}^H\mathbf{V}_1\boldsymbol{\Sigma}^{-1}\mathbf{U}_1^H\mathbf{G}]^{-1}\mathbf{b}. \tag{17}$$

V. Frequency Invariant Flat Top Beamformer

The proposed approach to design a flat top beampattern for a fixed frequency ω_k is to minimize the maximum error between the desired beampattern $\mathbf{y}(u,v)$ and the adapted beampattern $\mathbf{S}(u,v)\mathbf{w}$ sampled over P angles on a discrete grid,

$$\min \max_{u,v} \quad \epsilon = \left|\mathbf{y}(u,v) - \mathbf{S}(u,v)\mathbf{w}\right|. \tag{18}$$

The $P \times 1$ desired beampattern $\mathbf{y}(u,v) = \mathbf{y}_R(u,v) + j\mathbf{y}_I(u,v)$ is a disc of radius μ centered at $(u=0, v=0)$ with $\mathbf{y}(u,v) = 1e^{j\nu}$ if $u^2+v^2 \leq \mu$ and 0 otherwise. The angle ν is a user selected phase angle. The rows of the $P \times N$ matrix $\mathbf{S}(u,v) = [\mathbf{s}(u_0,v_0)|\ldots|\mathbf{s}(u_{P-1},v_{P-1})]^H$ are P steering vectors corresponding to the sampled spatial directions and $\mathbf{w}$ is the $N \times 1$ complex adaptive weight vector to be computed. The matrix $\mathbf{S}$ is complex so that $\mathbf{S} = \mathbf{S}_R + j\mathbf{S}_I$ and has rank equal to N which implies $P \geq N$.

Define the $2P \times 1$ real vector $\overline{\mathbf{y}} = \left[\mathbf{y}_R^T, \quad \mathbf{y}_I^T\right]^T$, the $2N \times 1$ real vector $\overline{\mathbf{w}} = \left[\mathbf{w}_R^T, \quad \mathbf{w}_I^T\right]^T$ and the $2P \times 2N$ real matrix

$$\overline{\mathbf{S}} = \begin{bmatrix} \mathbf{S}_R & -\mathbf{S}_I \\ \mathbf{S}_I & \mathbf{S}_R \end{bmatrix}. \tag{19}$$

Then minimizing the l_∞ norm in $\mathbb{C}^N$ of the complex error in (18) is equivalent to minimizing the l_∞ norm in $\mathbb{R}^{2P}$ of the real error

$$\min \max_{u,v} \quad \bar{\epsilon} = \left|\overline{\mathbf{y}} - \overline{\mathbf{S}}\overline{\mathbf{w}}\right|. \tag{20}$$

Equation (20) implies that

$$-\delta \leq \overline{\mathbf{y}} - \overline{\mathbf{S}}\overline{\mathbf{w}} \leq \delta \tag{21}$$

where $\delta \geq 0$ is a nonnegative scalar to be minimized. Equivalently,

$$\begin{aligned} \overline{\mathbf{S}}\overline{\mathbf{w}} - \delta &\leq \overline{\mathbf{y}}, \\ -\overline{\mathbf{S}}\overline{\mathbf{w}} - \delta &\leq -\overline{\mathbf{y}}. \end{aligned} \tag{22}$$

Rewriting (22) using matrix notation yields the optimization problem in standard form,

$$\begin{aligned} \min \quad & \begin{bmatrix} 0 & 0\ldots0 & 1 \end{bmatrix} \begin{bmatrix} \overline{\mathbf{w}} \\ \delta \end{bmatrix} \\ \text{such that} \quad & \begin{bmatrix} \overline{\mathbf{S}} & -\mathbf{1} \\ -\overline{\mathbf{S}} & -\mathbf{1} \end{bmatrix} \begin{bmatrix} \overline{\mathbf{w}} \\ \delta \end{bmatrix} \leq \begin{bmatrix} \overline{\mathbf{y}} \\ -\overline{\mathbf{y}} \end{bmatrix}. \end{aligned} \tag{23}$$

The real and imaginary parts of $\mathbf{w}$ are unrestricted free variables. Therefore, they can be written as the difference of two nonnegative numbers,

$$\begin{aligned} \mathbf{w}_R &= \mathbf{w}_R^+ - \mathbf{w}_R^- \\ \mathbf{w}_I &= \mathbf{w}_I^+ - \mathbf{w}_I^- \\ \mathbf{w}_R^+,\ \mathbf{w}_R^-,\ \mathbf{w}_I^+,\ \mathbf{w}_I^- &\geq 0. \end{aligned} \tag{24}$$

Now the linear optimization program in eqn. (23) can be rewritten in standard form as

$$\begin{aligned} \min \quad & \widehat{\mathbf{c}}^T\widehat{\mathbf{z}} \\ \text{such that} \quad & \widehat{\mathbf{A}}\widehat{\mathbf{z}} \leq \widehat{\mathbf{b}}, \\ & \widehat{\mathbf{z}} \geq \mathbf{0} \end{aligned} \tag{25}$$

where

$$\widehat{\mathbf{A}} = \begin{bmatrix} \mathbf{S}_R & -\mathbf{S}_R & -\mathbf{S}_I & \mathbf{S}_I & -\mathbf{1} \\ \mathbf{S}_I & -\mathbf{S}_I & \mathbf{S}_R & -\mathbf{S}_R & -\mathbf{1} \\ -\mathbf{S}_R & \mathbf{S}_R & \mathbf{S}_I & -\mathbf{S}_I & -\mathbf{1} \\ -\mathbf{S}_I & \mathbf{S}_I & -\mathbf{S}_R & \mathbf{S}_R & -\mathbf{1} \end{bmatrix}_{4P \times (4N+1)} \tag{26}$$

$$\widehat{\mathbf{z}} = \begin{bmatrix} \mathbf{w}_R^{+T} & \mathbf{w}_R^{-T} & \mathbf{w}_I^{+T} & \mathbf{w}_I^{-T} & \delta \end{bmatrix}^T_{(4N+1)\times 1}$$

$$\widehat{\mathbf{b}} = \begin{bmatrix} \mathbf{y}_R{}^T & \mathbf{y}_I{}^T & -\mathbf{y}_R{}^T & -\mathbf{y}_I{}^T \end{bmatrix}^T_{4P\times 1}$$

$$\widehat{\mathbf{c}} = \begin{bmatrix} 0 & 0 & \ldots & 0 & 1 \end{bmatrix}^T.$$

To solve the linear optimization program in (25), the nonnegative slack variables m^+ and m^- are introduced

$$\begin{aligned} \min \quad & \sum_{k=1}^{4P} m_k^+ + \sum_{k=1}^{4P} m_k^- \\ \text{such that} \quad & \widehat{\mathbf{A}}\widehat{\mathbf{z}} + \mathbf{Im}^+ - \mathbf{Im}^- = \widehat{\mathbf{b}}, \\ & \widehat{\mathbf{z}},\ \mathbf{m}^+,\ \mathbf{m}^- \geq \mathbf{0}. \end{aligned} \tag{27}$$

The slack variables m^+ and m^- transform the original inequality constraints in eqn. (25) into equality constraints and the new linear program to solve becomes

$$\begin{aligned} \min \quad & \widetilde{\mathbf{c}}^T\mathbf{p} \\ \text{such that} \quad & \widehat{\mathbf{A}}\widehat{\mathbf{z}} + \mathbf{Im}^+ - \mathbf{Im}^- = \widehat{\mathbf{b}}, \\ & \widehat{\mathbf{z}},\ \mathbf{m}^+,\ \mathbf{m}^- \geq \mathbf{0} \end{aligned} \tag{28}$$

where

$$\widetilde{\mathbf{c}} = \begin{bmatrix} \underbrace{0\ldots0}_{4N} & 0 & \underbrace{1\ldots1}_{2P} & \underbrace{0\ldots0}_{2P} & \underbrace{0\ldots0}_{2P} & \underbrace{1\ldots1}_{2P} \end{bmatrix}^T, \tag{29}$$

$$\mathbf{p} = \begin{bmatrix} \widehat{\mathbf{z}}^T & \mathbf{m}^{+T} & \mathbf{m}^{-T} \end{bmatrix}^T_{(4N+8P+1)\times 1}.$$

The linear program defined in (28) can be solved in a few iterations using optimizaton solvers such as Matlab *linprog*.

VI. Measured Results and Conclusion

Fig. 3 shows the U-principal plane versus frequency (dB scale) for the Adapted Pencil beampattern. The width of the main beam is very nearly constant over the entire 13.5 GHz bandwidth and the sidelobe levels are substantially reduced (-13.2 vs -30 dB) compared to the unadapted beampatterns shown in Fig. 2. Fig. 4 illustrates the array response in the direction $(u=0.4, v=0.3)$ versus frequency and demonstrates that the frequency invariant beamformer reduces the peak-to-peak frequency deviations by approximately 1 dB over the 13.5 GHz bandwidth. Fig. 5 illustrates U-principal plane cuts for the flat top beampattern centered at boresight. This beampattern is held perfectly fixed for the entire 13.5 GHz bandwidth.

The blue curve in Fig. 6 illustrates a measured PDP obtained using true time delay beam steering in the direction $(u=0.4, v=0.3)$ with an unadapted beampattern. These data were collected in a highly reflective utility plant environment with many metal surfaces and fixtures. There is a clear

multipath fading profile with a duration of approximately 35 nsec that corresponds to many superimposed multipath reflections arriving from random directions. This energy is primarily received through the sidelobes of the beampattern and is not confined to the angular width of the main beam. The multipath fading profile shown in red for a frequency invariant pencil beam appears diminished due to the reduced sidelobes of the beampattern.

Fig. 7 compares the measured frequency responses in the same direction with and without the adapted beamformer. With an unadapted beampattern, the frequency response appears nearly flat and noise-like due to the contributions of the received diffuse multipath energy. After applying the frequency invariant pencil beampattern, the frequency response of the beam output is much more band limited since the long duration multipath fading has been attenuated by the lower sidelobes of the beamformer.

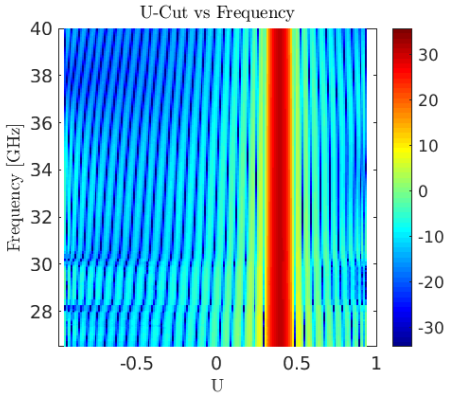

Fig. 3. U-Cut of Adapted Pencil beampattern.

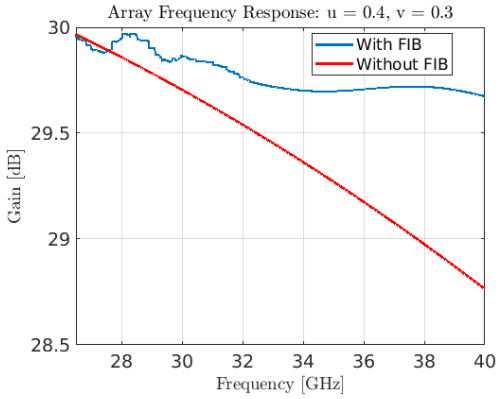

Fig. 4. Array Frequency Response: $(u = 0.4, v = 0.3)$.

REFERENCES

[1] M. G. Becker, B. Jamroz, K. A. Remley, P. Vouras, R. Jones, D. F. Williams, "Characterization and Uncertainty Analysis of a Spatial-Channel Test Environment for Wireless Over-the-Air Measurements," in print for *IEEE Transactions on Microwave Theory and Techniques*.

[2] P. Vouras, "Sample Support Requirements for Nonlinear Adaptive Beamforming," *Proceedings of the 49th Annual Conference in Information Sciences and Systems (CISS)*, March 2015.

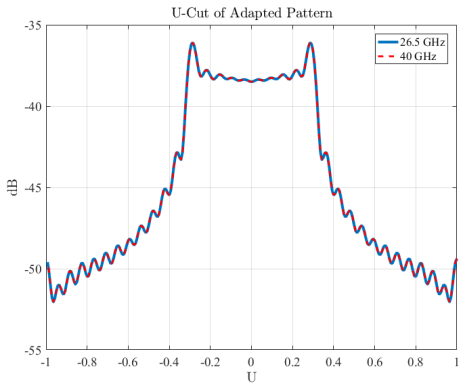

Fig. 5. U-Cut of Adapted Flat Top beampattern.

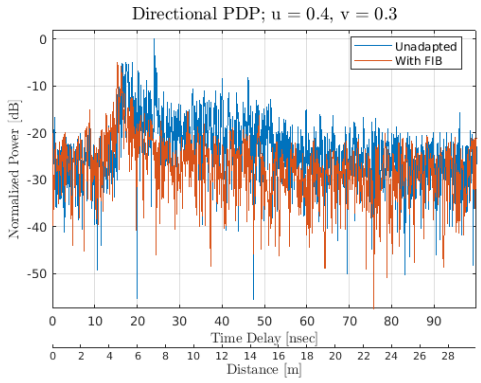

Fig. 6. Directional PDP Comparison: $(u = 0.4, v = 0.3)$.

[3] Y. Zhao, W. Liu, R. J. Langley, "Subband design of fixed wideband beamformers based on the least squares approach," *Elsevier Journal of Signal Processing*, September 29, 2010.

[4] D. P. Scholnik, J. O. Coleman "Optimal Array-Pattern Synthesis for Wideband Digital Transmit Arrays," *IEEE Journal of Selected Topics in Signal Processing*, Vol. 1, No. 4, December 2007.

[5] R. Sun, C. A. Gentille, J. Senic, P. Vouras, P. B. Papazian, N. T. Golmie, K. A. Remley, "Millimeter-Wave Radio Channels vs Synthetic Beamwidth," *IEEE Communications Magazine*, Vol. 56, Issue 12, 2018.

[6] R. L. Haupt, *Antenna Arrays: A Computational Approach*, John Wiley and Sons, Hoboken, NJ., 2010.

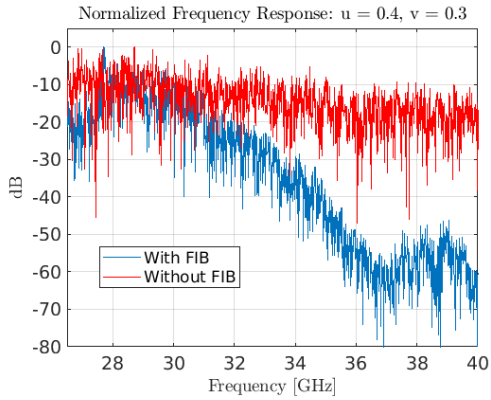

Fig. 7. Frequency Response Comparison: $(u = 0.4, v = 0.3)$.